# Small polarons mediated near-room-temperature metal–insulator transition in vanadium dioxide and their hopping dynamics

Xiongfang Liu,[1#] Tong Yang, [2#] Jing Wu,[3] Mengxia Sun,[1] Mingyao Chen,[1] Chi Sin Tang,[1,3,4*] Kun Han,[5] Difan Zhou,[1] Shengwei Zeng,[3,6] Shuo Sun,[1] Sensen Li[7], Ming Yang,[2*] Mark B.H. Breese,[4,6] Chuanbing Cai,[1] Thirumalai. Venkatesan,[8] Andrew T. S. Wee,[6,9] Xinmao Yin[1*]

[1]Shanghai Key Laboratory of High Temperature Superconductors, Shanghai Frontiers Science Center of Quantum and Superconducting Matter States, Physics Department, Shanghai University, Shanghai 200444, China

[2]Department of Applied Physics, The Hong Kong Polytechnic University, Kowloon, Hong Kong, China

[3]Institute of Materials Research and Engineering, A*STAR (Agency for Science, Technology and Research), 2 Fusionopolis Way, Singapore, 138634 Singapore

[4]Singapore Synchrotron Light Source (SSLS), National University of Singapore, Singapore 117603

[5]Information Materials and Intelligent Sensing Laboratory of Anhui Province, Institutes of Physical Science and Information Technology, Anhui University, Hefei 230601, China

[6]Department of Physics, Faculty of Science, National University of Singapore, Singapore 117542

[7]Department of Electronic Engineering, School of Electronic Science and Engineering, Xiamen University, Xiamen 361005, China

[8]Center for Quantum Research and Technology, University of Oklahoma, Norman, Oklahoma 73019, USA

[9]Centre for Advanced 2D Materials and Graphene Research, National University of Singapore, Singapore 117546

*Corresponding author
slscst@nus.edu.sg (C.S.T.)

*Corresponding author
kevin.m.yang@polyu.edu.hk (M.Y.)

*Corresponding author
yinxinmao@shu.edu.cn (X.Y.)

**Abstract:**

In the pursuit of advanced photoelectric devices, researchers have uncovered near room-temperature metal-insulator transitions (MIT) in non-volatile $VO_2$. Although theoretical investigations propose that polaron dynamics mediate the MIT, direct experimental evidence remains scarce. In this study, we present direct evidence of the polaron state in insulating $VO_2$ through high-resolution spectroscopic ellipsometry measurements and first-principles calculations. We demonstrate that polaron dynamics play a complementary role, working alongside Peierls and Mott transitions to contribute to the MIT processes. Moreover, our observations and characterizations of conventional metallic plasmons and Mott-like strongly-correlated plasmons in the respective phases of the $VO_2$ film provide valuable insights into their quantum electronic structures. The diverse quasiparticle dynamics underscore the interplay between quantum degrees of freedom and offer crucial evidence of how quantum correlated effects influence phase transitions in strongly-correlated systems. These findings not only enrich our understanding of the underlying mechanisms but also pave the way for developing novel device functionalities.

**Introduction:**

Strongly-correlated electronic systems is the key concept in condensed matter physics. Quantum many-body effects coupled with charge, orbital, spin and lattice degrees of freedom give rise to a rich family of nontrivial critical phenomena such as high-temperature superconductivity[1], symmetry-breaking phenomena[2], charge-density wave order[3, 4]. Specifically, metal-insulator transition (MIT) phenomenon in Mott insulators[5] emerges as the quintessential feature amongst the various quantum mechanical effects. MIT can be manipulated via multiple methods including carrier density modulation[6], orbital occupancy[7] and photo-induction[8, 9]. The MIT properties render a diverse range of quantum materials to be utilized in many applications related to energy-efficient systems[10], neuromorphic devices[8] and radiative thermal memristors[11]. However, complex strongly-correlated electronic systems present a challenge especially in the attempt to identify the underlying physical mechanism governing the MIT processes, which to date, remains to be understood.

The emergence of small polarons in strongly-correlated system is the key cornerstone to unlock the fundamental understanding of the quantum phenomena in such strongly-correlated systems. Given the strong influence of charge-lattice coupling effects, the onset of MIT and its underlying mechanism may fundamentally be mediated by the system's small polarons dynamics[12]. Besides, small polarons are virtually ubiquitous in diverse transition metal oxide[13, 14] and their ability to induce drastic changes which in turn drives and regulates corresponding structural and electronic phase transition processes are notable. Thus, an in-depth investigation on how small polarons dynamics would be an effective strategy in unlocking the MIT mechanism.

Vanadium dioxide ($VO_2$) serves as an ideal platform for the detailed investigation of small polarons dynamics. An archetypical non-volatile Mott insulator, it presents a first-order MIT[15] at room temperature accompanied by an abrupt change in resistivity by several orders of magnitude[16, 17] and structural distorted of V-atom chains[18]. Such MIT properties at room temperature endow $VO_2$ system with theoretical values and

application values. Notably, first-principles calculation have predicted the formation of small polarons in $VO_2$ along with their possible influence on its MIT properties[19, 20, 21]. However, a detailed understanding and direct experimental evidence of MIT effects induced by small polarons in $VO_2$ system remain largely elusive.

Here, we report the stabilization of small polarons in the insulating $VO_2$ by combining high-resolution spectroscopic ellipsometry measurements and extensive first-principles studies. In addition, metallic and correlated plasmon dynamics have been observed for portraying diagram of electronic structures and enriching quasiparticle pictures in polymorphic $VO_2$. Our studies reveal that decreasing temperature enhances the electron-phonon coupling in $VO_2$ which in turn leads to the concurrent onset of small polarons formation and Peierls lattice distortion. Subsequently, the enhancement of Mott electronic correlations brought about by a weakened screening effect with lower free electron population. The small polarons act as an intermediary to facilitate both the Peierls and Mott phase transitions processes in regulating the MIT processes of $VO_2$, as depicted in Fig. 1(a). The identification of a hybrid mechanism of Peierls and Mott transitions synergistically mediating the MIT processes provides a deep understanding of the actual MIT mechanisms, not only for $VO_2$, but also for a broad range of strongly-correlated oxides[22].

## Results

### Validation of Sample Quality

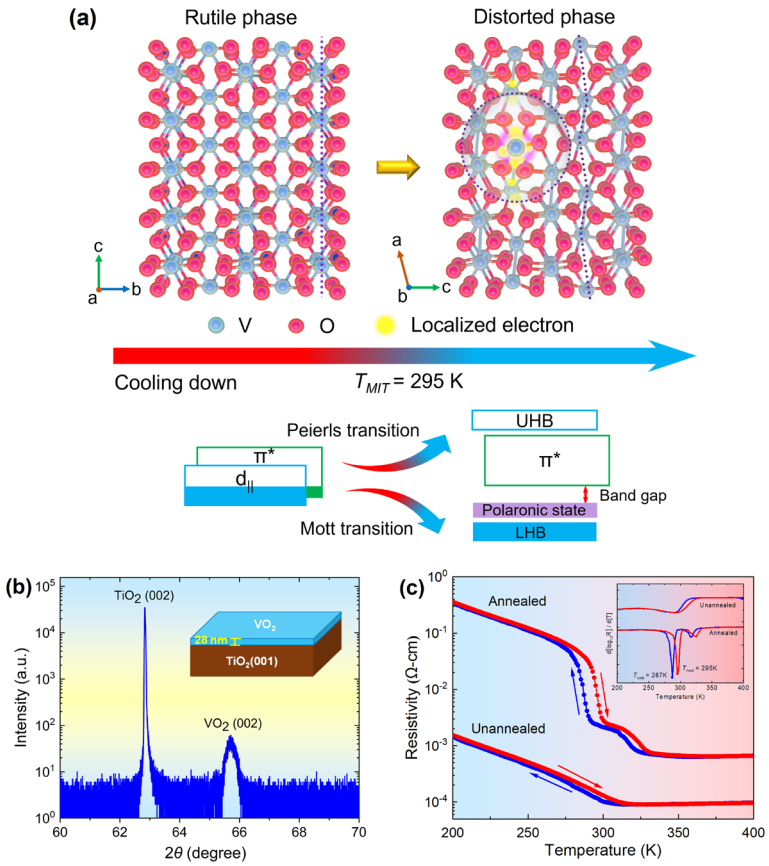


Figure 1. (a) Schematic depiction of the small polarons act as an intermediary to facilitate both the Peierls and Mott phase transitions processes in regulating the MIT processes of $VO_2$. (b) Structural analysis of epitaxial $VO_2$ thin film. XRD characterizations on $VO_2$ thin film grown on $TiO_2$ (001) substrate. $\theta$-$2\theta$ scan around the $TiO_2$ (002) and $VO_2$ (002) peak, no other peaks were found. (c) Resistance vs temperature curves for transport properties of annealed and unannealed $VO_2$ thin films grown on $TiO_2$ (001) substates. The inset shows the corresponding $d[\log_{10}(R)]/d[T]$ curves.

The $VO_2$ thin film was prepared on $TiO_2$ substrate by pulsed laser deposition (PLD). The thickness of the grown $VO_2$ layer was measured to be 28 nm. X-ray Diffraction (XRD) analyses and transport measurements were conducted on $VO_2/TiO_2$ films to confirm the high film and crystalline quality of the samples. Fig. 1(b) displays the X-

ray Diffraction (XRD) pattern of the 28 nm-$VO_2$/ $TiO_2$(001) sample, in which the 002-plane displayed features both the rutile $TiO_2$ substrate and the tetragonal-like $VO_2$ thin film located at 2θ =62.832° and 2θ =65.706°, respectively. The crystal quality of the thin film was further examined by X-ray Rocking Curve measurement (Supplementary material Fig. S2), further confirming the high crystallinity of the annealed $VO_2$ thin film.

Transport measurements are further conducted on the $VO_2/TiO_2$(001) system [Fig. 1(c)]. The metal−insulator transition (MIT) temperature and lineshape of the annealed $VO_2$ thin film are in good agreement with previous studies[23, 24, 25]. The resistivity of annealed $VO_2$ thin film is measured to be $6.7\times10^{-4}$ Ω·cm in metallic phase at 350 K. Resistivity increases by three orders of magnitude with decreasing temperature in the insulating phase. The resistivity of annealed $VO_2$ thin film is $1.2\times10^{-1}$ Ω·cm at 250 K. This two-step phase transition behavior is attributed to a slight oxygen-deficiency in the $VO_2$ film [26], which introduced extra electrons to the system [27]. As shown in the inset of Fig. 1(c), the MIT temperature ($T_{MIT}$) of annealed $VO_2$ film during the heating cycle is 295 K. While MIT takes place at 287 K during the cooling process with a small thermal hysteresis width of 8 K. As for the unannealed $VO_2$ with significantly higher oxygen vacancy concentration, it merely displays a semi-metallic behavior without any onset of MIT (see supplementary material). Annealed $VO_2/TiO_2$ sample with an abrupt transition by three orders of magnitude further affirms that our $VO_2$ sample is of high quality.

**Temperature-dependent Spectroscopic Ellipsometry Characterization**

Spectroscopic ellipsometry represents a versatile tool for probing the quasiparticle dynamics of strongly-correlated materials and it is widely utilized to establish the optical response and electronic structures at the nanoscale [28, 29]. Optical characterization of quasiparticles was conducted on the annealed-$VO_2/TiO_2$ film using spectroscopic ellipsometry at temperatures between 200 K and 350 K where the MIT takes place.

Optical response on the $VO_2$ film was collected with incident photon energy between 0.68 and 4.80 eV. With transport measurements confirming the MIT phenomena of the $VO_2$ film during the heating and cooling processes, it behaves as an insulator with a band gap (~0.6 eV) below 295 K ($T_{MIT}$) [11, 30], Whereas, it transforms into a rutile metal above 295 K[31]. These transport properties have been confirmed by the optical characterization using spectroscopic ellipsometry with prominent changes to the optical parameters caused by the transition process especially with regards to its energy bands and quasiparticle dynamics in both the metallic and insulating states. In the spectroscopic ellipsometry measurements, we observe the traces of three types of quasiparticles excitations, small polarons, metallic plasmons and correlated plasmons, respectively. The presence of polaron state related to small polarons is detected by analyzing the $\sigma_1$ absorption peaks in the insulating state. Next, metallic plasmons and correlated plasmons are found to distribute in the Electron Energy Loss Spectra (EELS). The properties of small polarons and plasmons are discussed in detail below, respectively.

## The Observation of Polaron state

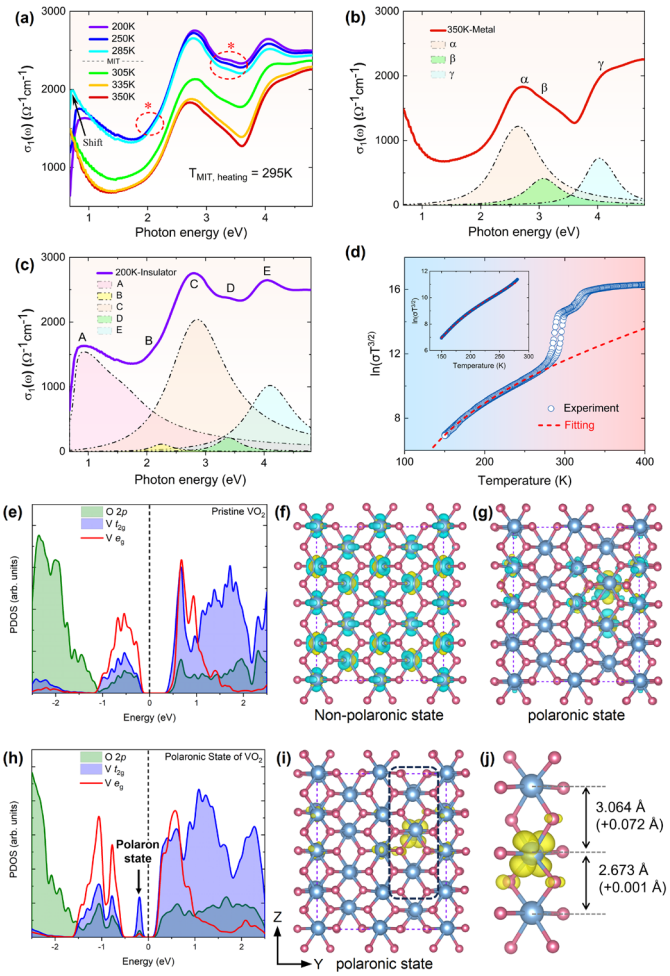


Fig. 2. (a) Optical conductivity of annealed $VO_2/TiO_2(001)$ film at various temperatures. (b) Optical conductivity curve of metallic $VO_2$ thin film (350 K), three independent peaks can be observed. (c) Optical conductivity curve of insulating $VO_2$ thin film (200 K), five independent peaks can be observed. (d) ln ($\sigma T^{3/2}$) vs T. The red dash line is fit to the data using the hopping conductivity of small polarons. Inset: ln ($\sigma T^{3/2}$) vs T, showing that activated behavior of small polarons is approximately followed only blow the $T_{MIT}$, with the same fitting line. (e) Projected density of states (PDOS) of pristine $VO_2$. (f-g). The charge density difference (f) between the non-polaron state and the charge-neutral state, and (g) between the polaron state and the charge-neutral state. The charge accumulation/depletion is denoted by the yellow/cyan iso-surface with an iso-value of (f) 0.0015 e/Å$^3$ and (g) 0.007 e/Å$^3$, respectively. (h) PDOS of $VO_2$ in the polaron state. The Fermi level has been set to 0 in both (e) and (h). (i) The visualized

partial charge density associated with the mid-gap state in (h). (j) The magnification of the localized charge enclosed in the black dashed rectangle of (e). The iso-value is set to 0.007 e/Å$^3$.

Figs. 2(a-c) display the optical conductivity, $\sigma_1(\omega)$, in the insulating (T=200 K, 250 K, 285 K) and the metallic states (T=305 K, 335 K, 350 K). The shape and spectral weight are different between the insulating and the metallic states. In the metallic phase at 350 K [Fig.2(b)], three peaks labelled α (~ 2.72 eV), β (~ 3.10 eV) and γ (~ 4.02 eV) can be observed and they can be modelled using five respective Gaussian peaks by Drude-Lorentz model (see supplementary material). The broad Drude response is a clear indication of the material's metallic nature[32, 33]. Combining with our analysis of spectroscopic ellipsometry, peak α (~ 2.72 eV) can be attributed to the transition from the filled O2p band to the half-filled $d_{||}$ band, while the weak shoulder peak β (~ 3.10 eV) is ascribed to the transition from the filled O2p band to the half-filled $\pi^*$ band. Meanwhile, peak γ is attributed to the transition between half-filled $d_{||}$ band and empty $\sigma^*$ band. These have been confirmed in previous studies [29, 34].

The onset of MIT at 295 K with the almost-simultaneous onset of Mott and Peierls transition [5, 35, 36, 37], lead to significant changes in both the optical conductivity and lattice structure. This in turn leads to a significant change to the $\sigma_1$ spectra below 295 K. In the insulating phase at 200 K [Fig. 2(c)], five peaks in optical conductivity can be observed. The temperature-dependent peak A (at ~ 0.92 eV at 200 K redshifts to ~ 0.76 eV at 285 K) is attributed to the transition between adjacent energy bands that near the Fermi level. Peak C at ~2.76 eV in the insulating phase can be attributed to the interband transition between the Lower Hubbard band (LHB) and Upper Hubbard band (UHB). The hump feature E at ~ 4.0 eV is due to the transition from the O2p band to the empty $\pi^*$ band and from LHB to empty $\sigma^*$ band[34] (see the supplementary material).

In addition to the previously established optical absorption features described above, two other previously unidentified features (labelled B and D) located at ~2.16 eV and ~3.40 eV, respectively, have been observed [Fig. 2(c)]. Intriguingly, the spectral weight of peak B and peak D are lower than the adjacent peaks. At 200 K, the maximum

spectral weight of peak B is ~114 $\Omega^{-1} \cdot cm^{-1}$ and the maximum spectral weight of peak D is ~214 $\Omega^{-1} \cdot cm^{-1}$. These features are also observed at other temperatures in the insulating phase. While their energy positions do no shift with rising temperature, they gradually weaken and eventually dissipate above the MIT temperature along with the formation of a Drude response in the metallic phase. Based on the energy positions and the relatively small spectral weight of peaks B and D, it can be deduced that they are attributed to the formation of a new narrow mid-gap state[38]. As discussed in detailed thereafter, we attribute feature B and D to the optical transitions from polaron state in the $VO_2$ film.

Due to the presence of a slight oxygen vacancy in annealing $VO_2$ film, the necessary conditions are created for the formation of small polarons which result from the coupling of excess electrons and phonons. It has been reported that the transport properties of insulating state $VO_2$ is dictated by the small polaron hopping dynamics, which in turn, is determined by the amplitude of the thermal lattice vibrations[39, 40]. Hence, the small polaron hopping model (see supplementary material) is utilized to model and confirm the presence of the small polarons in insulating $VO_2$. The electronic transport curve displayed in Fig. 2(d) shows that it is in good agreement with the theoretical small polaron hopping model in the insulating phase below $T_{MIT}$ (295 K). Whereas, the transport data begins to deviate from the theoretical model in the metallic state above $T_{MIT}$. This provides strong evidence that while small polaron are present in insulating phase $VO_2$, they begin to dissipate in metallic state $VO_2$ due to the increase in thermal lattice vibration above $T_{MIT}$.

Having provided experimental evidence that small polarons are present in the insulating state $VO_2$ based on the analysis of our electronic transport data, it is essential to attribute features B and D observed in the optical spectra (Fig. 2(c)) to the presence of the polaron state. While a previous theoretical study has indicated that polaron states are formed at energy region in the order of ~1 eV below the conduction band minimum (CBM)[41] in large bandgap oxide systems. With the relatively small bandgap of insulating $VO_2$, at ~ 0.6 eV, the formation of the small polaron state at 0.32 eV below the empty $\pi^*$ band at 200 K [Fig. 4(b)] is not only theoretically consistent, but also

agrees with experimental detected polaron state in other small bandgap oxide system[13]. Hence, we can now confirm features B (~ 2.16 eV) and D (~ 3.40 eV) in the optical conductivity ($\sigma_1$) spectra [Fig. 2(c)] to be optical transitions from the polaron state to the UHB and $\sigma^*$ band, respectively.

First-principles calculations have been performed to further substantiate the experimental evidence that the mid-gap state is attributed to the formation of small electron polarons. Fig. 2(e) displays the projected density of states (PDOS) of the pristine $VO_2$ at the GGA+U level of theory. The calculated band gap is 0.601 eV, in agreement with that previously reported for the insulating phase of $VO_2$ [11, 30]. When excess electrons are introduced, DFT calculations indicate that the non-polaron state [Fig. 2(f)] is 0.771 eV higher in energy than the polaron state [Fig. 2(g)], indicative of the energetic preference to the formation of the polaron state. Fig. 2(g) shows that the excess electrons in the polaron state is self-trapped around a vanadium site. Meanwhile, a neighboring vanadium site was also found to denote electrons to the host vanadium site. As illustrated in Fig. 2(h), a mid-gap state (marked by arrow) arises below the Fermi level in the polaron state, which is mainly composed of the V $t_{2g}$ states. The visualized partial charge density associated with this mid-gap state further confirms the localized nature of the excess electron [Fig. 2(i)]. Specifically, the shape of the partial charge density implies that the excess electron mainly occupies the V $3d_{yz}$ and $3d_{xz}$ orbitals [Fig. 2(j)]. Compared to the non-polaron state, the charge trapping further increases the long V-V distance, whereas the short V-V distance nearly remains unchanged, probably due to the aforementioned charge transfer from that neighboring V site. These DFT results are consistent with our experimental finding that the mid-gap state is attributed to the polaron state, which provides compelling experimental evidence for stabilization of small polarons.

**The Observation of Plasmons Excitations**

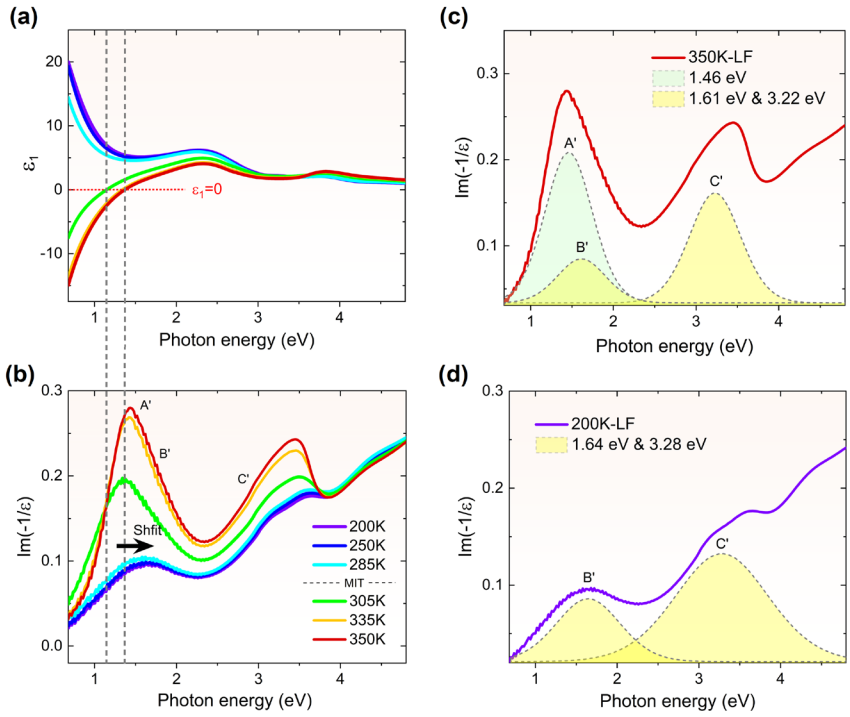


Fig. 3. (a) The real part of dielectric function ($\varepsilon_1$) at different temperatures. (b) The LF shows the character of metallic plasmons and correlated plasmons. The black arrow indicates peak A′ (metallic plasmons) shift to high-energy position as the temperature increases. (c) LF spectra of 350 K (metallic state) with identified peaks A′, B′ and C′. The position of peak B′ and C′ show two-fold energy positions relation. (d) LF spectra of 200 K (insulating state) with identified peaks B′ and C′ with two-fold energy positions relation.

To further analyze the quasiparticle features and opto-electronic properties of the $VO_2$ system and distinguish between the insulating and metallic phases, the optical loss function (LF) is further derived with the spectra displayed in Fig. 3 (see supplementary material). Metallic phase $VO_2$ shows clear metallic behavior with the prominent Drude response in $\sigma_1$ [Fig. 2(a)] and zero-crossing of $\varepsilon_1$ [Fig. 3(a)] at ~ 1.13 eV at 305 K. This zero-crossing blueshifts monotonically to ~ 1.37 eV at 350 K – near the energy position of loss-function peak A′ [Fig. 3(b)] marking the presence of metallic plasmons (peak A′) attributed to the collective excitation of free charges. Meanwhile,

the slight disparity between the $\varepsilon_1$ zero-crossing positions and their corresponding energy positions of loss-function peak A′ in the metallic state, as shown in Figs. 3(a-b), is attributed to free electron scattering[28].

Using Voigt profile fitting for the LF spectra for metallic phase $VO_2$, another two peaks labelled B′ and C′ at ~ 1.61 eV and ~ 3.22 eV, respectively at 350 K, are elucidated [Fig. 3(c)]. The positions of these two relatively weaker peaks follow a two-fold photon energy relation which persists throughout the entire temperature range. Besides, they are located in the photon energy region where the corresponding $\varepsilon_1$ spectra is the positive range. Note also that peak C′ generally has a higher peak intensity and its peak width is consistently wider than peak B′. These collective features of peaks B′ and C′ are signatures of correlated plasmonic excitations[42, 43, 44] where they arise due to the presence of strong electron−electron and electron−hole interactions in the $VO_2$ thin film. The analysis of the LF spectra and the presence of features A', B' and C' in metallic phase $VO_2$ provides clear evidence that both metallic and correlated plasmons coexist in this state.

The Intensity of peak A' attributed to the metallic plasmon register a corresponding drop with decreasing temperature and it dissipates in the insulating phase below $T_{MIT}$. Meanwhile, both features B' and C' belonging to the correlated plasmon prevail where their intensity and peak positions remain generally consistent throughout [Fig. 3(d)] (see supplementary material). The dissipation of metallic plasmon feature A' marks the transformation of the $VO_2$ film from the metallic to the insulating state below $T_{MIT}$ [45, 46]. Meanwhile, the high-energy features above 3.5 eV in the LF spectra may be attributed to electronic interband transitions in both metallic and insulating phases[47, 48].

**Proposed Mechanism Between Small Polarons and MIT Processes**

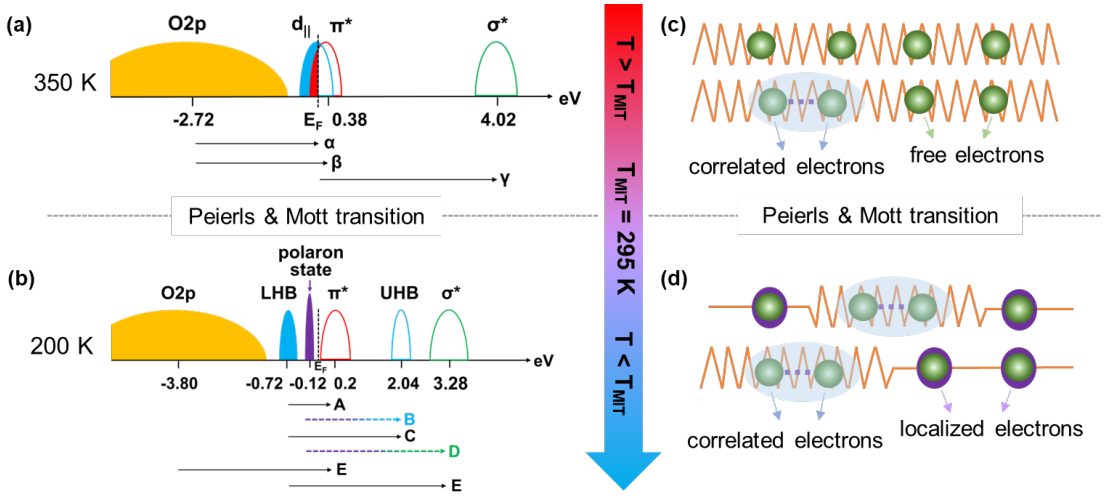


Fig. 4. Pictorial models of the energy level for (a) metallic state at 350 K, (b) insulating state at 200 K, showing the relevant oxygen and vanadium energy levels. The arrows in (a-b) denote interband transitions in good agreement with our values for corresponding features in Figs. 2(b-c), respectively. Fermi level is denoted by $E_F$. (c-d) Schematic diagrams of the electronic states during the MIT transition of $VO_2$ system. (c) In the metallic state of $VO_2$, the electrons are delocalized. The metallic matrix exhibits collective oscillations of free electrons and correlated electrons. (d) As the temperature decreases, the number of correlated electrons increases, and the delocalized electrons transform into localized electrons. Therefore, correlated electrons and small polarons are present in the insulating state. The transition from metallic to insulating states in $VO_2$ is a result of a combination of lattice distortions (Peierls transition), electronic correlation effects (Mott transition), and the opening of a band gap.

Previous X-ray Absorption Spectroscopic (XAS) studies [49, 50] have described the energy positions of unoccupied V-3d bands. In its insulating state, $\pi^*$, UHB and $\sigma^*$ band locate above the Fermi level (see supplementary material). As detailed on the origin of features in Figs. 2(a-c), features from electronic transitions have been defined in the previous section of this study (the Observation of Polaron state). Therefore, the energy band schematics in the metallic (350 K) and insulating (200 K) states can be depicted in Figs. 4(a-b) by combining results of previous XAS characterization studies and the

optical transitions derived from our optical conductivity data. As discussed previously, feature B has been attributed to the electronic transition from polaron state to UHB, while feature D is attributed to electronic transition from polaron state to $\sigma^*$ band. The important characteristic for the polaron state is shown clearly in the insulating phase.

Having confirmed the presence of small polarons and by analyzing the temperature-dependent energy band properties, this provides a new perspective on how small polarons facilitate the MIT processes and open the bandgap in the $VO_2$ film which is yet to be fully understood. Figs. 4(c-d) provide a pictorial representation of the quantum electronic structures and phase transition processes. In the high-temperature metallic phase, the effects of thermal lattice vibration outweigh the effect of electron localization[51]. Meanwhile, the excitations of free and correlated charges (metallic and correlated plasmons) further prevent the localization of the electron due to their periodic motion. Such high-temperature electron dynamics prevent the formation of small polarons. However, as temperature decreases and as it approaches $T_{MIT}$, there is a corresponding weakening of the thermal lattice vibrations which in turn result in the gradual enhancement of electron-phonon interaction. It facilitates the formation of small polarons which is typically accompanied by a series of lattice distortion and lattice symmetry breaking due to the localization of electrons[52] in the vicinity of the V-lattice sites. Such structural distortions provide an important condition which in turn facilitate its phase transition process in the form of a Peierls transition[53, 54]. Meanwhile, in another proposed phase transition -Mott theory - which describes the motion of electrons in the $V(3d_{||})$-$V(3d_{||})$ channels[55], there is a significant reduction in free electrons as they become localized at the V lattice sites to form small polarons. The reduction of free electrons significantly weakens the electronic screening effect and this reinforces the system's electronic correlations especially at low temperature[55, 56, 57, 58]. As a result, it forms an insulating state via the opening of an energy gap as evidenced in the low-temperature metal-insulator transition as described by the Mott theory. Having highlighted the important complementary role that small polarons can play in mediating both the Peierls structural transition and the Mott electronic phase transition processes, we can thereby suggest that small polarons serve as an important

intermediary in facilitating a hybrid mechanism comprising the aforementioned phase transitions in $VO_2$.

## Discussion

In conclusion, our optical observations couple with DFT calculations provide clear evidence of small polarons in $VO_2$ and by analyzing its temperature-dependent behavior in both the metallic and insulating phases. This brings about a new perspective in unravelling the MIT mechanism that underlies this strongly-correlated electronic system. The understanding of the role that polaron dynamics play is pivotal to understanding charge transport properties in $VO_2$. Besides, it provides a link to unravel how structural kinetics and electronic properties play a complementary role in the MIT process of strongly-correlated electronic system. In fact, the genuinely development of quantum many-body theory is company with study and understand the complexity of quasiparticles. Following and inspecting many-body effects and quasiparticles dynamics in strongly-correlated oxides allow for potential applications related to energy conversion, such as thermoelectric generators, Peltier elements and photoelectric devices. Hence, regulating quasiparticles generation and dynamics is undoubtedly advantageous to gadget performance.

## Method

### Sample preparation and Annealing

$VO_2$ thin films of thickness 28 nm were synthesized on $TiO_2$(001) substrates (CrysTec GmbH) by Pulsed Laser Deposition (PLD). A commercial vanadium single crystal (100)-orientated metal target with 99.999 % purity (Goodfellow) has been used as the target for synthesis of the $VO_2$ films. Deposition process of the $VO_2$ films on the $TiO_2$(001) substrates take place at an optimized pressure and temperature of $10^{-3}$ Torr and 400 ℃, respectively with a pulse laser repetition rate of 5 Hz. After the synthesis process, one of the $VO_2/TiO_2$ film was then annealed in oxygen at $10^{-3}$ Torr pressure at temperature 600 ℃ to improve the sample quality and to remove any existing oxygen

vacancies. Meanwhile, as a reference to the annealed sample, the other $VO_2/TiO_2$ film is kept unannealed.

**X-ray Diffraction and Electron Transport Measurements**

X-ray Diffraction (XRD) pattern and X-ray Rocking Curve measurement were operated using a SmartLab system with a 2θ range from 60 to 70° in step of 0.05°. The electron transport data were taken using the standard four-probe method in a commercial Quantum Design physical property measurement system (PPMS).

**Spectroscopic Ellipsometry Measurements**

Spectroscopic ellipsometry (SE) measurements are conducted using a custom-made Variable Angle Spectroscopic Ellipsometer (VASE) of J. A. Woollam Co., Inc in the photon energy range of 0.68-4.80 eV at incident angles of 70° with respect to the plane normal.

**The first-principles calculations**

All density functional theory (DFT) calculations were carried out using the Vienna ab initio Simulation Package (VASP) with the projector augmented-wave method and the Perdew-Burke-Ernzerhof (PBE) parameterized Generalized Gradient Approximation (GGA) adopted for the ion-electron interaction and the exchange-correlation interaction, respectively.

**Data availability**

The data that support the findings of this study are available within the article and its Supplementary Information. Additional relevant data are available from the corresponding authors upon reasonable request.

**Acknowledgements**

This work was supported in part by the Strategic Priority Research Program of the Chinese Academy of Sciences, Grant No. XDB25000000, National Natural Science Foundation (52172271), the National Key R&D Program of China No.

2022YFE03150200, Shanghai Science and Technology Innovation Program (22511100200). S.S.L. would like to thank the funding support from National Natural Science Foundation of China (NSFC) (No. 62175206). M.Y. acknowledges the funding support from The Hong Kong Polytechnic University (project number: 1-BE47, ZE0C, ZE2F and ZE2X).

**Author contributions**

X.L., T.Y. contributed equally to this work. X.Y. conceived the project. K.H., S.Z., T.V synthesized the samples and K.H., S.Z. performed the electron transport experiments and analyzed the data, C.S.T. performed the XRD experiments and analyzed the data and X.L., C.S.T., M.S., S.S.L., M.C. performed the SE experiments and analyzed the data. T.Y., M.Y. performed the DFT calculations. X.L. and C.S.T. wrote the manuscript, with input from all the authors.

**Competing interests**

The authors declare no competing interests.

**Correspondence** and requests for materials should be addressed to Chi Sin Tang or Ming Yang or Xinmao Yin.

**References**

1. Han S*, et al.* Orbital-Hybridization-Driven Charge Density Wave Transition in CsV(3) Sb(5) Kagome Superconductor. *Adv Mater* **35**, 2209010 (2022).

2. Singh CN, Piper LFJ, Paik H, Schlom DG, Lee W-C. Correlation-induced emergent charge order in metallic vanadium dioxide. *Phys Rev B* **105**, 035150 (2022).

3. Chavez-Cervantes M*, et al.* Charge Density Wave Melting in One-Dimensional Wires with Femtosecond Subgap Excitation. *Phys Rev Lett* **123**, 036405 (2019).

4. Lahneman DJ*, et al.* Insulator-to-metal transition in ultrathin rutile VO2/TiO2(001). *NPJ Quantum Mater* **7**, (2022).

5. Haverkort MW*, et al.* Orbital-assisted metal-insulator transition in VO2. *Phys Rev Lett* **95**, 196404 (2005).

6. Kim H-T, Kim B-J, Lee YW, Chae B-G, Yun SJ, Kang K-Y. Hole-driven MIT theory, Mott transition in VO2, MoBRiK device. *Physica C* **460-462**, 1076-1078 (2007).

7. Aetukuri NB*, et al.* Control of the metal–insulator transition in vanadium dioxide by modifying orbital occupancy. *Nat Phys* **9**, 661-666 (2013).

8. Li G*, et al.* Photo-induced non-volatile VO2 phase transition for neuromorphic ultraviolet sensors. *Nat Commun* **13**, 1729 (2022).

9. Johnson AS*, et al.* Ultrafast X-ray imaging of the light-induced phase transition in VO2. *Nat Phys* **19**, 215-220 (2022).

10. Li M, Magdassi S, Gao Y, Long Y. Hydrothermal Synthesis of VO2 Polymorphs: Advantages, Challenges and Prospects for the Application of Energy Efficient Smart Windows. *Small* **13**, 1701147 (2017).

11. Cheng S*, et al.* Inherent stochasticity during insulator-metal transition in VO(2). *PNAS* **118**, 2105895118 (2021).

12. Franchini C, Kresse G, Podloucky R. Polaronic hole trapping in doped BaBiO3. *Phys Rev Lett* **102**, 256402 (2009).

13. Smart TJ, Pham TA, Ping Y, Ogitsu T. Optical absorption induced by small polaron formation in transition metal oxides: The case of Co3O4. *Phys Rev Mater* **3**, 102401(R) (2019).

14. Wickramaratne D, Bernstein N, Mazin II. Role of defects in the metal-insulator transition in VO2 and V2O3. *Phys Rev B* **99**, 214103 (2019).

15. Liu M*, et al.* Terahertz-field-induced insulator-to-metal transition in vanadium dioxide metamaterial. *Nature* **487**, 345-348 (2012).

16. Li L*, et al.* Manipulating the insulator-metal transition through tip-induced hydrogenation. *Nat Mater* **21**, 1246-1251 (2022).

17. Han K*, et al.* Enhanced Metal-Insulator Transition in Freestanding VO2 Down to 5 nm Thickness. *ACS Appl Mater Interfaces* **13**, 16688-16693 (2021).

18. Xu C*, et al.* Transient dynamics of the phase transition in VO(2) revealed by mega-electron-volt ultrafast electron diffraction. *Nat Commun* **14**, 1265 (2023).

19. B.Goodenough J. The Two Components of the Crystallographic Transition in VO2*. *J Solid State Chem* **3**, 490-500 (1971).

20. Lysenko S, Vikhnin V, Rúa A, Fernández F, Liu H. Critical behavior and size effects in light-induced transition of nanostructuredVO2films. *Phys Rev B* **82**, 205425 (2010).

21. Mott NF. Metal-Insulator Transition. *Rev Mod Phys* **40**, 677-683 (1968).

22. Franchini C, Reticcioli M, Setvin M, Diebold U. Polarons in materials. *Nat Rev Mater* **6**, 560-586 (2021).

23. Hu K*, et al.* Thickness-dependent anisotropy of metal-insulator transition in (110)-VO2 /TiO2 epitaxial thin films. *J Alloys Compd* **699**, 575-580 (2017).

24. Muraoka Y, Hiroi Z. Metal–insulator transition of VO2 thin films grown on TiO2 (001) and (110) substrates. *Appl Phys Lett* **80**, 583-585 (2002).

25. Paik H*, et al.* Transport properties of ultra-thin VO2 films on (001) TiO2 grown by reactive molecular-beam epitaxy. *Appl Phys Lett* **107**, 163101 (2015).

26. Lee. J, C.B.Eom. Isostructural metal-insulator transition in VO2. *Science* **362**, 1037–1040 (2018).

27. Yin W-J, Wen B, Zhou C, Selloni A, Liu L-M. Excess electrons in reduced rutile and anatase TiO2. *Surf Sci Rep* **73**, 58-82 (2018).

28. Yin X*, et al.* Quantum Correlated Plasmons and Their Tunability in Undoped and Doped Mott-Insulator Cuprates. *ACS Photonics* **6**, 3281-3289 (2019).

29. Qazilbash MM*, et al.* Electrodynamics of the vanadium oxidesVO2andV2O3. *Phys Rev B* **77**, 115121 (2008).

30. Wei J, Wang Z, Chen W, Cobden DH. New aspects of the metal-insulator transition in single-domain vanadium dioxide nanobeams. *Nat Nanotechnol* **4**, 420-424 (2009).

31. Bahrami M, Vasilopoulos P. RPA Plasmons in Graphene Nanoribbons: Influence of a VO(2) Substrate. *Nanomaterials* **12**, 2861 (2022).

32. Horng J*, et al.* Drude conductivity of Dirac fermions in graphene. *Phys Rev B*

**83**, 165113 (2011).

33. Li ZQ*, et al.* Dirac charge dynamics in graphene by infrared spectroscopy. *Nat Phys* **4**, 532-535 (2008).

34. Li WW, Yu Q, Liang JR. Intrinsic evolutions of optical functions, band gap, and higher-energy electronic transitions in VO2 film near the metal-insulator transition region. *Appl Phys Lett* **99**, 241903 (2011).

35. Koethe TC*, et al.* Transfer of spectral weight and symmetry across the metal-insulator transition in VO(2). *Phys Rev Lett* **97**, 116402 (2006).

36. Yao T*, et al.* Understanding the nature of the kinetic process in a VO2 metal-insulator transition. *Phys Rev Lett* **105**, 226405 (2010).

37. Biermann S, Poteryaev A, Lichtenstein AI, Georges A. Dynamical singlets and correlation-assisted Peierls transition in VO2. *Phys Rev Lett* **94**, 026404 (2005).

38. Nagatsuka N, Kato K, Wilde M, Fukutani K. Absence of midgap states due to excess electrons donated by adsorbed hydrogen on the anatase TiO2(101) surface. *Phys Rev B* **105**, 045424 (2022).

39. Zhong X, LeClair P, Sarker SK, Gupta A. Metal-insulator transition in epitaxial VO2thin films on TiO2(100). *Phys Rev B* **86**, 094114 (2012).

40. Andreev VN, Klimov VA. Electrical conductivity of the semiconducting phase in vanadium dioxide single crystals. *Phys Solid State* **49**, 2251-2255 (2007).

41. Reticcioli M, Diebold U, Kresse G, Franchini C. Small Polarons in Transition Metal Oxides. In: *Small Polarons in Transition Metal Oxides*) (2020).

42. Ferrara DW, Nag J, MacQuarrie ER, Kaye AB, Haglund RF, Jr. Plasmonic probe of the semiconductor to metal phase transition in vanadium dioxide. *Nano Lett* **13**, 4169-4175 (2013).

43. Ayral T, Biermann S, Werner P. Screening and nonlocal correlations in the extended Hubbard model from self-consistent combinedGWand dynamical mean field theory. *Phys Rev B* **87**, 125149 (2013).

44. Ayral T, Werner P, Biermann S. Spectral properties of correlated materials: local vertex and nonlocal two-particle correlations from combined GW and dynamical mean field theory. *Phys Rev Lett* **109**, 226401 (2012).

45. Kana Kana JB, Vignaud G, Gibaud A, Maaza M. Thermally driven sign switch of static dielectric constant of VO 2 thin film. *Opt Mater* **54**, 165-169 (2016).

46. Gentle A, Maaroof AI, Smith GB. Nanograin VO2in the metal phase: a plasmonic system with falling dc resistivity as temperature rises. *Nanotechnology* **18**, 025202 (2007).

47. Thomas M, Chain EE. Optical properties and electron energy-loss diagnostics of vanadium dioxide thin films. *Thin Solid Films* **204**, L1-L4 (1991).

48. Bianconi A, Stizza S, Bernardini R. Critical behavior of the plasmon resonance at the metal-insulator transition in VO2. *Phys Rev B* **24**, 4406-4411 (1981).

49. Ruzmetov D, Senanayake SD, Ramanathan S. X-ray absorption spectroscopy of vanadium dioxide thin films across the phase-transition boundary. *Phys Rev B* **75**, 195102 (2007).

50. Kumar M, Kim Y, Lee HH. Temperature dependent structural, electrical and electronic investigation of VO2 (B) thin film. *Curr Appl Phys* **30**, 85-90 (2021).

51. Zibrov IP, Filonenko VP, Sidorov VA, Chtchelkatchev NM, Magnitskaya MV. Synthesis, structure and transport properties of high-pressure modification VO2(S). *Materialia* **23**, 101456 (2022).

52. Johannes MD, Hoang K, Allen JL, Gaskell K. Hole polaron formation and migration in olivine phosphate materials. *Phys Rev B* **85**, 115106 (2012).

53. Cavalleri A, Dekorsy T, Chong HHW, Kieffer JC, Schoenlein RW. Evidence for a structurally-driven insulator-to-metal transition inVO2: A view from the ultrafast timescale. *Phys Rev B* **70**, 161102 (2004).

54. Gervais F, Kress W. Lattice dynamics of oxides with rutile structure and instabilities at the metal-semiconductor phase transitions of NbO2 and VO2. *Phys Rev B* **31**, 4809-4814 (1985).

55. Yeo LH*, et al.* Anomalous spectral-weight transfers unraveling oxygen screening and electronic correlations in the insulator-metal transition ofVO2. *Phys Rev B* **91**, 081112(R) (2015).

56. Okazaki K, Sugai S, Muraoka Y, Hiroi Z. Role of electron-electron and electron-phonon interaction effects in the optical conductivity ofVO2. *Phys Rev B* **73**, 165116 (2006).

57. Zylbersztejn A, Mott NF. Metal-insulator transition in vanadium dioxide. *Phys Rev B* **11**, 4383-4395 (1975).

58. Rusydi A*, et al.* Electronic screening-enhanced hole pairing in two-leg spin

ladders studied by high-resolution resonant inelastic x-ray scattering at Cu M edges. *Phys Rev Lett* **113**, 067001 (2014).